Electrostatic Self-Calibration of Vibratory Gyroscopes

G. Casinovi, W. K. Sung, M. Dalal, A. N. Shirazi and F. Ayazi

IEEE International Conference on Micro Electro Mechanical Systems
pp. 559–562, January 2012

Abstract

This paper introduces a new approach to self-calibration of Coriolis-based vibratory gyroscopes that does not require the use of any additional moving parts or a calibration stage. Instead, the effect of the Coriolis force on the device is mimicked by the application of a rotating excitation to the device drive and sense modes. This calibration method is based on the theoretical analysis of an equivalent 2-DOF mass-spring model, which can be used to describe the behavior of a variety of MEMS gyroscopes. The method is validated both by the results of finite-element simulations and by experimental measurement.

Copyright Notice

ELECTROSTATIC SELF-CALIBRATION OF VIBRATORY GYROSCOPES

G. Casinovi, W.K. Sung, M. Dalal, A. N. Shirazi and F. Ayazi
Georgia Institute of Technology, Atlanta, Georgia, USA

ABSTRACT

This paper introduces a new approach to self-calibration of Coriolis-based vibratory gyroscopes that does not require the use of any additional moving parts or a calibration stage. Instead, the effect of the Coriolis force on the device is mimicked by the application of a rotating excitation to the device drive and sense modes. This calibration method is based on the theoretical analysis of an equivalent 2-DOF mass-spring model, which can be used to describe the behavior of a variety of MEMS gyroscopes. The method is validated both by the results of finite-element simulations and by experimental measurement.

INTRODUCTION

On-chip self-calibration of a gyroscope is a valuable feature that can eliminate expensive and time consuming mechanical calibration of the device using rate tables and address any long term drift of its scale factor. In recent years a number of self-test and self-calibration techniques for gyroscopes [1,2] and accelerometers [2,3] have appeared in the literature. A common feature to those techniques is the incorporation of a mobile platform of some sort (e.g. a rotary stage) in the sensor die to perform the calibration. In contrast, the approach to self-calibration of Coriolis-based vibratory gyroscopes presented in this paper does not require the use of any additional moving parts or calibration stage. Instead, the effect of the Coriolis force is mimicked by the application of a rotating excitation to the drive and sense resonance modes of the device. Specifically, it will be shown that under appropriate excitation conditions the Coriolis force created by a rotation around the gyroscope axis induces a phase shift in the gyroscope vibration pattern — and consequently in its output — that is directly proportional to the rotation rate Ω_z. It will also be shown that the application of a rotating excitation to the gyroscope drive and sense modes creates a similar phase shift in the device output, which is also proportional to the rotation rate of the excitation. It follows that a rotating excitation, which can be created by a rotating electrostatic field applied to the device electrodes, can be substituted for physical rotation for calibration purposes.

This self-calibration method requires a novel sensor readout architecture in which both the sense and drive modes of the gyroscope are excited at the same time. This differs from currently used readout schemes, in which only the drive mode is excited. The rotation rate Ω_z is read out by measuring the phase shift in the device output (e.g. the output current at any of the gyro electrodes).

THEORETICAL ANALYSIS

The self-calibration method presented in this paper is based on the analysis of an equivalent 2-DOF mass-spring model of vibratory gyroscopes [4]. The analysis that follows compares the gyroscope response to the Coriolis force caused by rotation to its response to a rotating excitation force when the gyroscope remains stationary in an inertial reference system.

Gyroscope Response to Coriolis Force

Assume first that a mode-matched gyroscope (i.e. $f_{drive} = f_{sense} = \omega_0/2\pi$) rotates around its z-axis (the sensitive axis) at a constant angular velocity Ω_z with respect to a fixed inertial frame of reference. Excitations that are 90° out of phase are applied to the two degenerate resonance modes of the device. Then the behavior of the gyroscope, modeled by its equivalent 2-DOF mass-spring system, is described by the following equations

$$\begin{aligned} \ddot{q}_1 + \frac{\omega_0}{Q}\dot{q}_1 - 2\lambda\Omega_z\dot{q}_2 + \omega_0^2 q_1 &= F_1\cos\omega_0 t \\ \ddot{q}_2 + \frac{\omega_0}{Q}\dot{q}_2 + 2\lambda\Omega_z\dot{q}_1 + \omega_0^2 q_2 &= F_2\sin\omega_0 t \end{aligned} \tag{1}$$

where (q_1,q_2) are generalized coordinates, ω_0 is the resonance frequency of the mass-spring systems, Q their quality factor, and λ a constant that depends on the gyroscope type and on the index of the resonance mode of the device [4]. The steady-state solution to this set of differential equations is found to be

$$\begin{aligned} q_1(t) &= \frac{Q}{\omega_0}\frac{\sqrt{(F_1\omega_0)^2 + (2F_2Q\lambda\Omega_z)^2}}{\omega_0^2 + (2Q\lambda\Omega_z)^2}\sin(\omega_0 t - \theta_1) \\ q_2(t) &= -\frac{Q}{\omega_0}\frac{\sqrt{(F_2\omega_0)^2 + (2F_1Q\lambda\Omega_z)^2}}{\omega_0^2 + (2Q\lambda\Omega_z)^2}\cos(\omega_0 t - \theta_2) \end{aligned} \tag{2}$$

where

$$\theta_1 = \tan^{-1}\frac{2F_2Q\lambda\Omega_z}{F_1\omega_0} \quad \theta_2 = \tan^{-1}\frac{2F_1Q\lambda\Omega_z}{F_2\omega_0} \tag{3}$$

The equations above show that the Coriolis force introduces phase delays θ_1 and θ_2 in the gyroscope response. For small values of Ω_z, these phase delays are directly proportional to Ω_z.

Gyroscope Response to Rotating Excitation

In this second analysis the gyroscope is assumed to be fixed in an inertial frame of reference. A sinusoidal excitation is applied to the gyroscope in such a way that the direction of the excitation rotates in the generalized coordinates plane at angular velocity Ω_z. As shown in Fig. 1, this is equivalent to applying amplitude-modulated excitations in the direction of the coordinate axes, which correspond to the two resonance modes of the device. Under these assumptions the behavior of the gyroscope is described by the following set of equations

$$\begin{aligned} \ddot{q}_1 + \frac{\omega_0}{Q}\dot{q}_1 + \omega_0^2 q_1 &= F_0\cos\Omega_z t\cos\omega_0 t \\ \ddot{q}_2 + \frac{\omega_0}{Q}\dot{q}_2 + \omega_0^2 q_2 &= F_0\sin\Omega_z t\cos\omega_0 t \end{aligned} \tag{4}$$

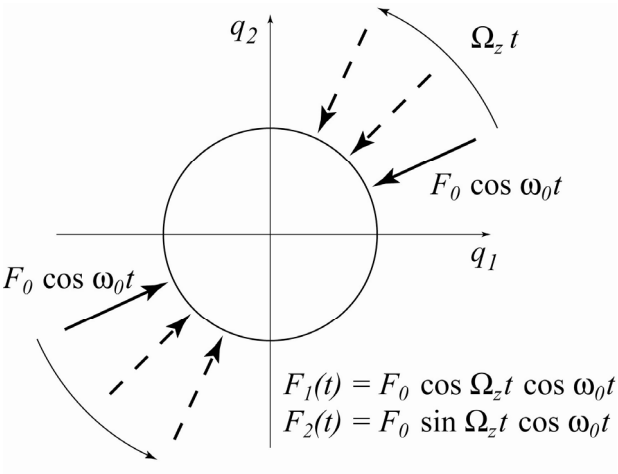

Figure 1: A rotating excitation is equivalent to amplitude-modulated excitations in the coordinate axial directions.

The two differential equations are now decoupled, and each can be solved independently of the other. The corresponding solutions can be obtained by exploiting the trigonometric identities

$$\cos\Omega_z t \cos\omega_0 t = \frac{1}{2}\left[\cos(\omega_0 + \Omega_z)t + \cos(\omega_0 - \Omega_z)t\right]$$

$$\sin\Omega_z t \cos\omega_0 t = \frac{1}{2}\left[\sin(\omega_0 + \Omega_z)t - \sin(\omega_0 - \Omega_z)t\right]$$

Standard sinusoidal steady-state analysis techniques, the details of which are omitted because of space reasons, can then be used to obtain expressions for the gyroscope response, which is determined by the following transfer function

$$H(j\omega) = \omega_0^2 - \omega^2 + j\frac{\omega_0}{Q}\omega$$

Assuming that $|\Omega_z| << \omega_0$, the following approximate equality holds

$$\left|H\left[j(\omega_0 + \Omega_z)\right]\right| \cong \left|H\left[j(\omega_0 - \Omega_z)\right]\right|$$

It can then be shown that the solutions of (4) are given by the following expressions

$$\begin{aligned} q_1(t) &= \frac{F_0}{A}\cos(\Omega_z t - \theta_0)\sin\omega_0 t \\ q_2(t) &= \frac{F_0}{A}\sin(\Omega_z t - \theta_0)\sin\omega_0 t \end{aligned} \qquad (5)$$

where

$$\begin{aligned} A &= \left|H\left[j(\omega_0 + \Omega_z)\right]\right| \cong \left|H\left[j(\omega_0 - \Omega_z)\right]\right| \\ \theta_0 &= \tan^{-1}\frac{2Q\Omega_z}{\omega_0} \end{aligned} \qquad (6)$$

Therefore the application of amplitude-modulated excitations to the drive and sense modes of the gyroscope induces a phase shift in the modulating envelope of the gyroscope response. For small values of Ω_z, this phase shift is proportional to Ω_z through a constant equal to $(2Q/\omega_0)$. Apart from a factor of λ, this is the same proportionality constant that relates the phase shift in the gyroscope response created by the Coriolis force to the rotation rate Ω_z (assuming $F_1 = F_2$). It follows that a rotating excitation can be substituted for physical rotation

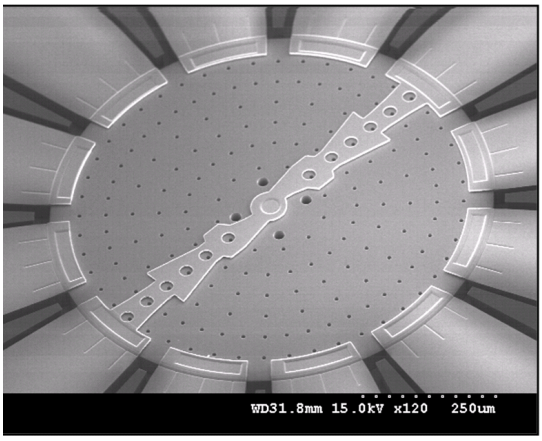

Figure 2: SEM picture of a disk BAW gyroscope.

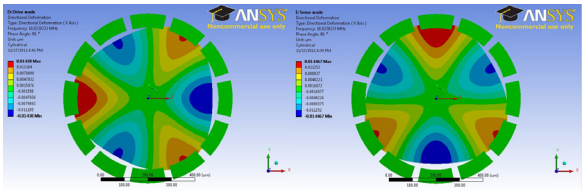

Figure 3: Drive (left) and sense (right) mode shapes of index n = 3 of a BAW disk gyroscope.

for the purpose of calibrating the gyroscope, because for a given type of gyroscope the value of λ depends only on the index of the resonance mode of the device.

Since the 2-DOF mass-spring model describes the behavior of a large class of resonating gyroscopes, the results of this analysis are applicable to a wide variety of devices, such as disk, ring, hemispherical shell and mode-matched tuning-fork gyroscopes.

NUMERICAL SIMULATIONS

The results of the theoretical analysis described in the previous section were verified by numerical simulations performed on an ANSYS model of a bulk acoustic wave (BAW) disk gyroscope of the same type as the one shown in Fig. 2 [5,6]. The gyroscope consists of a center-supported disk structure with capacitively-coupled drive, sense and control electrodes. Its mode of operation was assumed to be the in-plane resonance mode of index $n = 3$ [5] (Fig. 3). This choice of mode of operation allows the gyroscope to be fabricated on a (100) silicon wafer, because the two degenerate resonance modes with this index are spatially 30° apart and therefore have the same resonance frequency, despite the anisotropic nature of single-crystal silicon.

A first set of simulations was used to evaluate the phase shift in the gyroscope response caused by the Coriolis force. In these simulations sinusoidal excitations at the resonance frequency of the mode were applied to a pair of electrodes aligned with the drive mode. Similar excitations of equal amplitude but 90° out of phase were applied to the pair of electrodes perpendicular to the first pair, which is aligned with the sense mode. The phases of the output currents at all the electrodes were recorded at eight different rotation rates, ranging from zero to 2100 °/s.

Figure 4 shows the changes in the phases of the

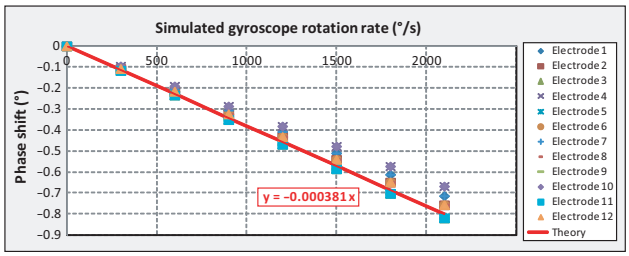

Figure 4: Simulated phase shift in the BAW disk gyro response due to the Coriolis force, measured relative to its value at zero rotation rate. The solid line shows the theoretical analysis predictions.

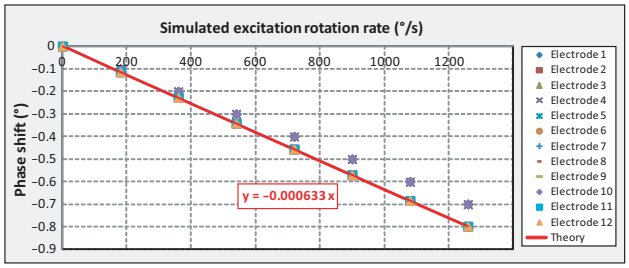

Figure 5: Simulated phase shift in the BAW disk gyro response due to a rotating excitation, measured relative to its value at zero rotation rate. The solid line shows the theoretical analysis predictions.

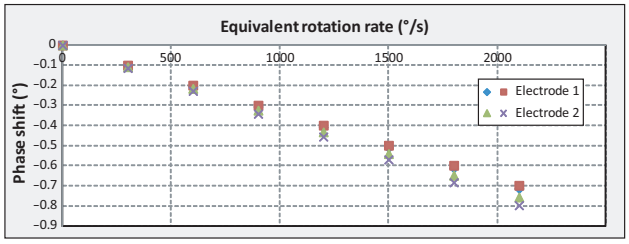

Figure 6: Comparison of the phase shifts in the gyroscope response due to the Coriolis force and a rotating excitation. The angular velocity of the rotating excitation has been rescaled by a factor of $(1/\lambda)$ with respect to Fig. 5.

electrode currents relative to their values at zero rotation rate. The theoretical relationship between phase shift and rotation rate given in (3) is shown in the figure by a solid line (assuming $F_1 = F_2$). It can be seen that the change in the phase shift in the response is almost identical at all the electrodes, and that the values obtained from the numerical simulations are in very good agreement with those derived from the theoretical analysis using $\lambda = 2n/(n^2+1) = 0.6$ [4]. The small differences in the slopes of the lines corresponding to different electrodes are due to the different DC polarization voltages applied to the electrodes in order to match the resonance frequencies of the drive and sense modes.

The gyroscope response to a rotating excitation — in this case, a rotating electrostatic field — was evaluated in a second set of simulations. In these simulations, amplitude-modulated excitations according to the expressions given in (4) were applied to the gyroscope electrodes aligned with the drive and sense modes. The phases of the output currents at all the electrodes were recorded at eight different values of the modulating angular frequency Ω_z, which in this case mimics the gyroscope rotation rate.

Figure 5 shows the changes in the phases of the electrode currents relative to their values at $\Omega_z = 0$, as well as the theoretical relationship given in (6) (solid line). In comparing the plots in Fig. 4 with those in Fig. 5, it should be kept in mind that the phase shifts at the same value of Ω_z differ by a factor of λ. When this factor is accounted for, the plots in the two figures essentially coincide, as shown in Fig. 6.

In summary, the simulation results confirm the relationship predicted by the theoretical analysis between the phase shift in the gyroscope response due to the Coriolis force and the phase shift created by a rotating excitation.

EXPERIMENTAL RESULTS

To further corroborate the results of both theoretical analysis and numerical simulations, measurements were taken on a mode-matched tuning-fork gyroscope [7] like the one shown in Fig. 7. This particular gyroscope was chosen because a vacuum-packaged device complete with control electronics was available for testing. A printed circuit board was designed so that the phase shift in the device response due to either a Coriolis force or an input rotating excitation could be measured.

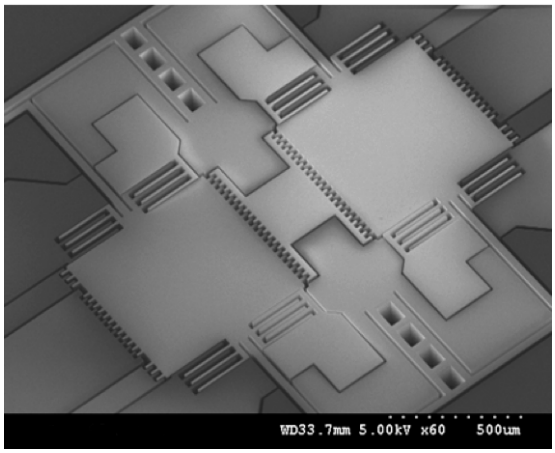

Figure 7: SEM view of a mode-matched tuning-fork gyro (M^2-TFG) [7].

To measure the phase shift induced by the application of a Coriolis force, an Agilent 4395A network analyzer was used to generate an input voltage at the resonance frequency of the device (ω_0). This signal was applied to the drive electrodes corresponding to one of the two degenerate resonance modes of the gyroscope (*I*-mode). An on-board phase shifter was used to generate a signal 90° out of phase with the input that was applied to the pair of drive electrodes corresponding to the other resonance mode (*Q*-mode). Two separate sense channels were used to amplify the *I* and *Q* output currents, after which the phase response was extracted through synchronous demodulation. Specifically, the output of the *I*-mode was mixed with the drive signal of the same mode to generate the following signal

$$s(t) = A\cos(\omega_0 t)\sin(\omega_0 t - \theta_1)$$

$$= \frac{A}{2}\left[\sin(2\omega_0 t - \theta_1) - \sin\theta_1\right]$$

The output and drive signals of the *Q*-mode were also

mixed in a similar way. Then the high-frequency components were eliminated using low-pass filters. Assuming that θ_1 and θ_2 are sufficiently small, the remaining DC components are proportional to Ω_z through the proportionality constants given in (3). A rate table was used to provide sinusoidally-varying rotation rates ranging from zero to 175 °/s. The corresponding measured phase shifts in the gyroscope response are shown in Fig. 8. It can be seen that the data points are aligned very closely along a straight line, as predicted by the theory.

A second set of measurements was then performed to analyze the gyroscope phase shift response to a rotating excitation. For this purpose, a low-frequency sinusoidal signal was applied to the phase shifter to generate in-phase and quadrature (90° out of phase) components. Both signals were independently mixed with a sinusoidal signal operating at the resonance frequency of the gyroscope to create the amplitude-modulated excitation sinusoids used to excite the *I* and *Q* drive electrodes, according to the expressions in (4). The output signal of each mode was again amplified along independent channels, but this time each was passed through a second demodulating stage that was needed to remove the $2\omega_0$ component created by the first demodulating stage. The output signal was filtered and averaged over 500 seconds to measure the phase-dependent DC shift resulting from the amplitude-modulated *I* and *Q* signals. The corresponding measured phase shifts in the gyroscope response are shown in Fig. 9. In this case, too, the data points are aligned fairly closely along a straight line.

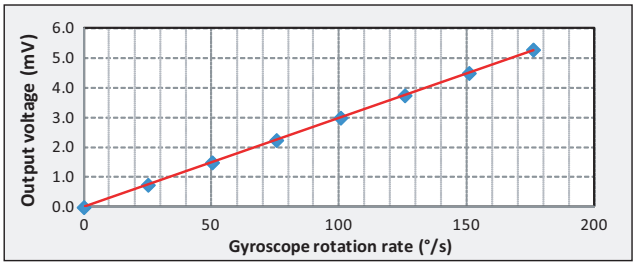

Figure 8: Measured phase shift in the M²-TFG response due to the Coriolis force, relative to its value at zero rotation rate. The solid line shows the best linear fit to the data.

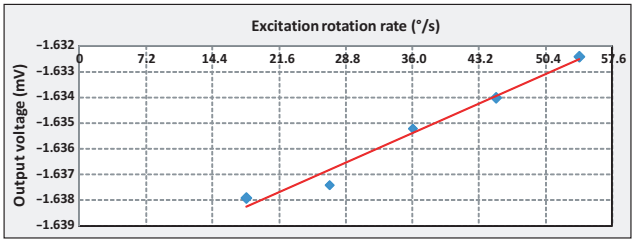

Figure 9: Measured phase shift in the M²-TFG response due to a rotating excitation, relative to its value at zero rotation rate. The solid line shows the best linear fit to the data.

CONCLUSIONS

The self-calibration method presented in this paper relies on a new sensor readout architecture in which two degenerate resonance modes of the gyroscope are excited at the same time. An analysis of the gyroscope behavior based on an equivalent 2-DOF mass-spring model predicts that the Coriolis force induces a phase shift in the gyroscope response. The analysis also predicts that this phase shift is directly related to the phase shift created by an excitation that rotates in the plane of the generalized coordinates corresponding to the two resonance modes of the device.

The very good agreement among theoretical analysis, finite-element simulations and experimental measurements proves the accuracy of the theoretical results and demonstrates that a rotating excitation can be substituted for physical rotation for the purpose of calibrating or self-testing the gyroscope.

ACKNOWLEDGEMENTS

This research work was supported by Qualtré, Inc.

REFERENCES

[1] T. Link *et al*, "A New Self-Test and Self-Calibration Concept for Micro-Machined Gyroscopes", in *Tech. Digest TRANSDUCERS'05 Conf.*, Seoul, Korea, June 5–9, 2005, pp. 401–404.

[2] K. Bauer *et al*, "Self-Test for Resonant Structure Sensors Applied to a Tuning Fork Gyro and a Resonant Accelerometer", in *Tech. Digest TRANSDUCERS'01 Conf.*, Munich, Germany, June 10–14, 2001, pp. 468–471.

[3] M. Aikele *et al*, "Resonant Accelerometer with Self-Test", *Sensors and Actuators A*, vol. 92, pp. 161–167, 2001.

[4] B. J. Gallacher *et al*, "Principles of a Three-Axis Vibrating Gyroscope", *IEEE Trans. Aerosp. Electron. Syst.*, vol. 37, pp. 1333–1343, 2001.

[5] H. Johari and F. Ayazi, "Capacitive Bulk Acoustic Wave Silicon Disk Gyroscopes", in *Tech. Digest 2006 IEDM*, San Francisco, CA, Dec. 10–13, 2006, pp. 513–516.

[6] W. K. Sung, M. Dalal and F. Ayazi, "A 3MHz Spoke Gyroscope with Wide Bandwidth and Large Dynamic Range", in *Tech. Digest 2010 IEEE MEMS Conf.*, Hong Kong, China, Jan. 24–28, 2010, pp. 104–107.

[7] M. F. Zaman, A. Sharma, Z. Hao and F. Ayazi, "A Mode-Matched Silicon-Yaw Tuning-Fork Gyroscope with Subdegree-Per-Hour Allan Deviation Bias Instability", *IEEE J. Microelectromech. Syst.*, vol. 17, pp. 1526–1536, 2008.

CONTACT

G. Casinovi, tel: +1-404-385-2454;
Giorgio.Casinovi@ece.gatech.edu